Available online at www.sciencedirect.com

SCIENCE DIRECT®

Sedimentary Geology 171 (2004) 91–111

Sedimentary Geology

www.elsevier.com/locate/sedgeo

Comparison of detrital zircon age distributions by kernel functional estimation

K.N. Sircombe[a,*], M.L. Hazelton[b]

[a]*Tectonics Special Research Centre, School of Earth and Geographical Sciences, University of Western Australia, M004, 35 Stirling Highway, Crawley, WA 6009, Australia*

[b]*School of Mathematics and Statistics, University of Western Australia, M019, 35 Stirling Highway, Crawley, WA 6009, Australia*

Received 1 September 2003; received in revised form 15 February 2004; accepted 12 May 2004

Abstract

A method is presented for assessing and statistically testing the similarity of detrital zircon U–Pb age distributions frequently used in provenance analysis, correlation and tectonic reconstructions. The method accounts for intrinsic measurement uncertainties by constructing kernel functional estimates of each set of age data that compensate for different degrees of measurement error by the application of varying levels of smoothing. The dissimilarity between these estimates can be quantified and provides a meaningful comparison between age distributions. A Monte Carlo permutation algorithm is used to test for equality between age distributions by grouping two sets of age data and then resampling the age distributions. The techniques are demonstrated with both synthetic and real data. Synthetic data illustrate the behaviour of the algorithms with data containing varying age modes and measurement uncertainties. Real data from Tasmania and southeastern Australia illustrates both the broad correlation with previous similarity assessment techniques and the applicability of the described methods to provenance, regional correlation and tectonic reconstruction.

Keywords: Zircon; Age distributions; Similarity; Kernel functional estimate; Permutation testing

1. Introduction

The U–Pb age of a detrital zircon from a sedimentary rock provides a proxy for the age of the igneous or metamorphic rock in which the zircon originally formed. Thus, the distribution of measured detrital zircon ages provides a record of the provenance of the sedimentary detritus. Detrital zircon geochronology has burgeoned recently with the advent of analytical systems that produce large sets of age data within reasonable timeframes. Some examples of the wide range of geological problems tackled are continental reconstruction (e.g. Rainbird et al., 1998; Cox et al., 1998; Berry et al., 2001),

* Corresponding author. Current address: Geoscience Australia, Curtin Geochronology Office, Department of Applied Physics, Curtin University of Technology, GPO Box U1987, Perth, WA 6845, Australia.

E-mail address: K.Sircombe@exchange.curtin.edu.au (K.N. Sircombe).

0037-0738/$ - see front matter © 2004 Elsevier B.V. All rights reserved.
doi:10.1016/j.sedgeo.2004.05.012

tectonism (e.g. Gehrels et al., 2002; DeGraaff-Surpless et al., 2003) and basin evolution (e.g. Cawood and Nemchin, 2000; Hallsworth et al., 2000).

The first stage of any interpretation of detrital zircon age distribution is a simple visual comparison of plotted data, typically univariate age distributions, with either the "known" ages of potential protosources or comparison with other age distributions and a judgment of "similarity". While the human eye is good at qualitatively recognizing similarities, it must be recognized that detailed interpretation based on simple visual comparison is always prone to subjective bias. Also, as the volume of data available for interpretation continues to grow, visual interpretations will diminish in utility. For instance, how does one, using visual inspection alone, meaningfully describe the similarity between 25 age distributions when there are 300 one-on-one comparisons? In cases such as continental reconstruction where the interpretation of similarities may have global impact, the need to objectively and quantifiably compare age distributions has become vital. Recently, a number of methods have been described to tackle this issue (Gehrels, 2000; Sircombe, 2000; Berry et al., 2001). While each has merit, they also have fundamental difficulties that devalue their application. A major challenge for any mathematical comparison is accounting for intrinsic measurement uncertainty. This is a notable problem where there is a need to compare age distributions resulting from a variety of analytical methods with markedly different precision.

Section 2 of this paper examines some previous methods before Section 3 develops a new method for assessing the similarity of age distributions that does account for measurement error. The methodology is based upon the construction of kernel functional estimates (Wand and Jones, 1995). Section 3 also describes how the similarity of functional estimates from different samples can be assessed and Section 4 explains how a Monte Carlo permutation test allows formal comparison of pairs of age distributions. Section 5 describes how clustering algorithms can be applied to the similarity results to illustrate relationships among samples. The algorithms described have been implemented in the R statistical and graphing package (Ihaka and Gentleman, 1996; Grunsky, 2002); the implementations are detailed in Appendix A. Both synthetic and real age data are used in Section 6 to illustrate the application of algorithms.

2. Previous methods

There are two approaches to more sophisticated comparisons of age distributions. The first approach is to deconvolve an age distribution to reveal individual age components and thereby make a comparison between those components. Examples of this approach for fission-track and U–Pb grain ages are detailed in Brandon (1992), Brandon and Vance (1992) and Sambridge and Compston (1994). Such deconvolution is a valuable tool for aiding the interpretation of complex age distributions and has been widely used. However, the inter-sample comparison of resolved age components may still rely on a qualitative assessment. For instance, deconvolution may reveal that one sample has age components (and 2σ errors) at 475 ± 10, 550 ± 12 and 1235 ± 30 Ma whereas a second sample has age components at 480 ± 5, 570 ± 10 and 1500 ± 40 Ma. A qualitative comparison would suggest that the first two components are "similar", although another interpreter may argue that the second components in each sample are barely within uncertainty of each other and the case for similarity is weak.

The second approach to the comparison of age distributions looks at the age distributions as a whole and deconvolution into components is not necessary. Gehrels (2000, p. 8) describes the concept of overlap and similarity between samples and established western North American references. Both overlap and similarity vary from 0 (no match) to 1 (perfect match). Overlap is defined as the presence of an age in both age distributions being compared (Gehrels et al., 2002, p. 205). Similarity is calculated by summing the square root of the product of each pair of probabilities (Gehrels, 2000, p. 8). While providing a quantification of similarity and aiding the interpretation of western North American provenance, this approach does not include a statistical test.

Berry et al. (2001) used the Kolmogorov–Smirnov (K–S) goodness-of-fit test to compare potential provenance similarities between Neoproterozoic and Cambrian sedimentary units in Tasmania, southern and southeastern Australia and North America. This

test takes the stepwise cumulative probability distribution of the measured ages and calculates a test statistic on the basis of the maximum distance between the distributions being compared. This provides a statistical basis for testing similarity, but the standard method does not account for age errors and tends to be less sensitive at extreme ends of the distribution (Press et al., 1988, p. 626) where complex detrital populations may be expected to differ the most.

Multivariate analysis has also been applied to large sets of detrital data in eastern Australia (Sircombe, 2000). Based on the age probability distributions, this approach proved useful in quantifying the effect of longshore drift on the detrital zircon age distributions without direct comparison with external references. However, the method is computationally complex and requires relatively large sets of data (e.g. 20+ samples of ~60 ages each) to avoid outliers having a strong influence.

3. Functional estimation

Imagine that there are two sites from which we are to collect data, and that the true age distributions of detrital zircon at the sites are described by the plots in Fig. 1a and b. In practice, each age sampled from one of these distributions will be subject to measurement error. Suppose that we collect data at site 1, and by chance those samples whose true age is less than 550 Ma are subject to measurement error with a standard deviation of 30 Ma, while those samples whose true age is greater than 550 Ma have measurement error

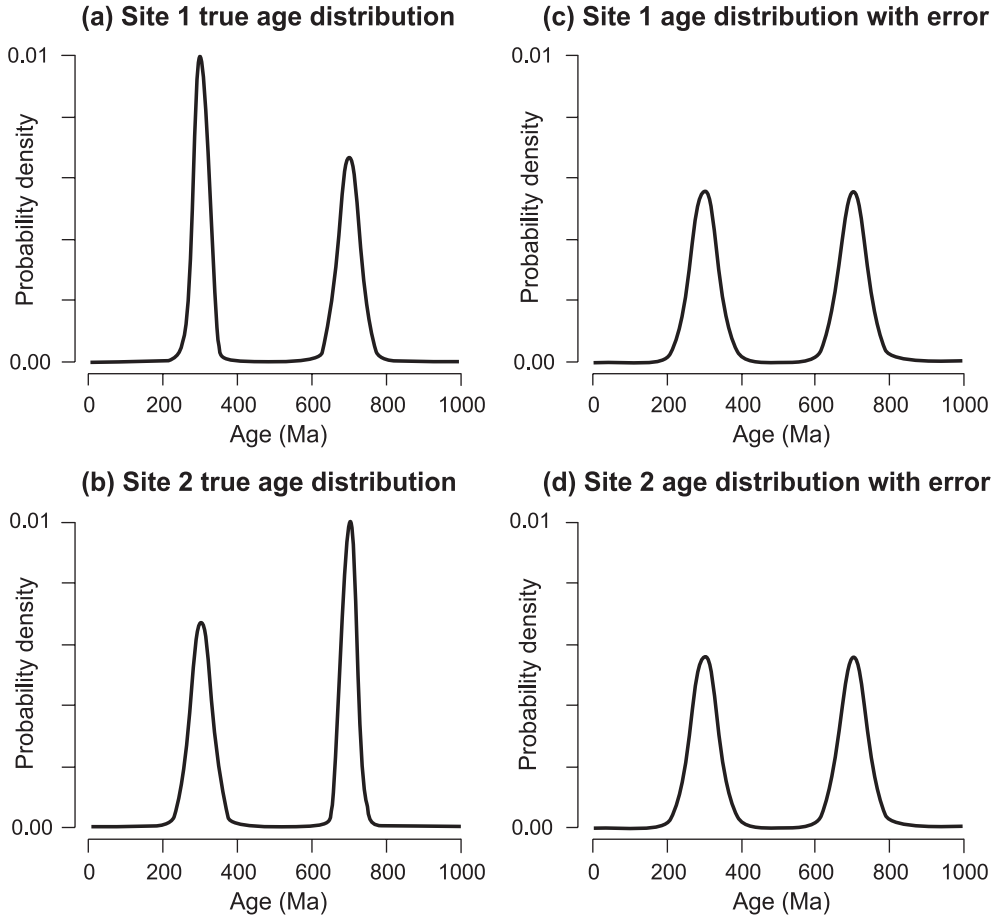

Fig. 1. (a, b) Density functions for distributions of true ages and (c, d) ages subject to measurement error, for two sites.

with standard deviation 20 Ma. Suppose that at site 2 the situation is reversed, with the samples younger than 550 Ma subject to measurement error with standard deviation of 20 Ma, and those older than 550 Ma having measurement error with standard deviation of 30 Ma. It can then be shown that the distributions of observed (i.e. error prone) ages from the two sites are as displayed in (Fig. 1c and d). They are identical. It follows that any methodology for comparing the age distributions at the two sites that ignores measurement error (e.g. the Kolmogorov–Smirnov test) will be completely powerless to detect any difference between them. Of course, this example is highly artificial, but it does illustrate the need for a method of comparison that takes account of measurement error.

In order to derive a method of comparison that does account for measurement error, we must introduce some notation. Consider data from a single site and let the random variable X denote a typical observed age. This age can be decomposed as $X=Y+Z$ where the random variable Y is the true age of the particular sample of detrital zircon in question, and the random variable Z represents measurement error.

We assume that the true age Y has a continuous probability distribution with probability density function (or simply *density* for short) f. If the sample was collected at site 1 as described above, for example, then this density f would be as displayed in Fig. 1a. We assume that the measurement error Z is normally distributed with mean zero and standard deviation σ, which we will refer to as the *measurement standard deviation*. We will denote the corresponding normal density (with mean zero and standard deviation σ) by ϕ_σ. An implicit assumption underlying the methodology that we now develop is that the probability density f represents faithfully the age distribution of interest. The sampling distribution of Y will not be a faithful representation of the true age distribution if grains are analysed on a qualitative basis of colour or morphology rather than a quantitative random selection (see Fedo et al., 2003). The method presented here is inapplicable for qualitative data and it is important to stress that some data in the literature will not be suitable for comparison using this method.

We will denote the density function for the observed age random variable X by g. If the measurement standard deviation varies as described in the opening paragraph of this section, then g for site 1 is displayed in Fig. 1c. In practice, we will assume that the measurement standard deviation for each observation is known, so that we may regard σ as fixed for each sampled age. In this case the density g, conditional on σ, is given by

$$g(x|\sigma) = \int f(y)\phi_\sigma(x-y)\mathrm{d}y \equiv f^*\phi_\sigma(x) \qquad (1)$$

where * denotes a convolution (as defined by the integral in the above equation) and ϕ_σ is a normal density as defined above. In the absence of detailed knowledge regarding the form of f, estimation of this true age density from error contaminated observations like X is a nonparametric deconvolution problem (Stefanski and Carroll, 1990). This type of problem is known to be very difficult, with good results often requiring millions of observations. It follows that comparison of two age distributions by direct estimation of their underlying density functions, f_1 and f_2, will typically be impractical. Nonetheless, we can hope to compare f_1 and f_2 by computing a measure of the distance between some transformed versions of the densities that is easier to estimate than the density function itself. As we show below, $f^*\phi_c$ is such a transformation of the true age density, where c is a constant to be determined.

Let $X_1,\ldots,X_n$ be a random sample of n observed ages from a particular site. The kernel density estimator (e.g. Wand and Jones, 1995) computed from these data is defined by

$$\hat{g}(x) = \frac{1}{n}\sum_{i=1}^{n} K_h(x-X_i) \qquad (2)$$

where $K_h(x)=K(x/h)/h$. Here the kernel K is a probability density function, and h is a smoothing parameter called the bandwidth. The standard normal density function is a popular choice of kernel, and turns out to be particularly appropriate in the present context because of its computational properties. Therefore we assume $K_h=\phi_h$ (i.e. a normal density with standard deviation h) henceforth. A pictorial illustration of a kernel density estimate constructed from four data points is given in Fig. 2a. Here the solid line is the density estimate itself, which is the aggregate of the individual kernel functions (each weighted to carry probability mass ¼) that are

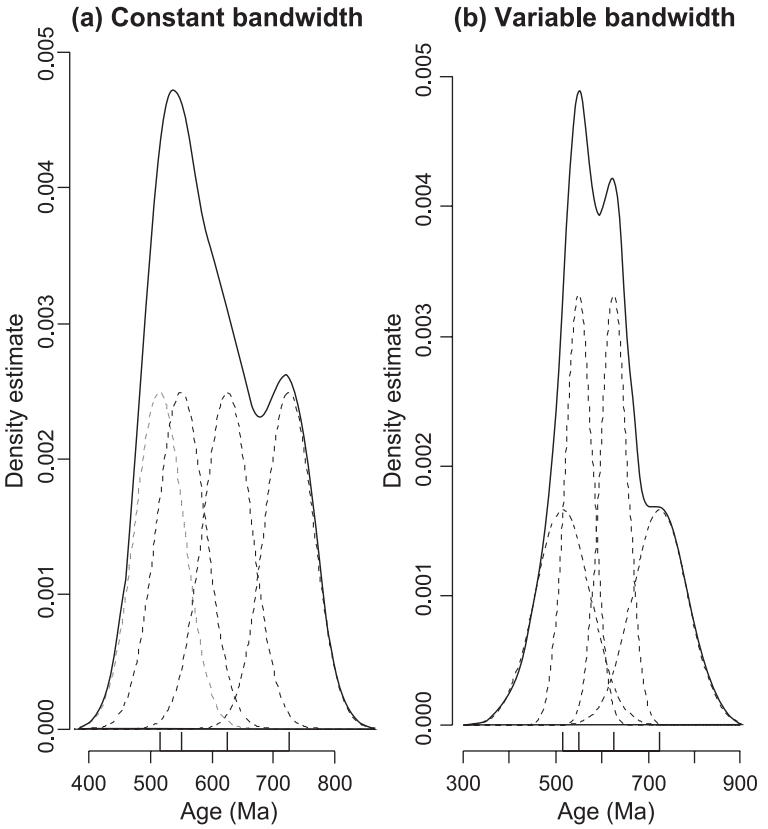

Fig. 2. Construction of kernel density estimates, depicting the individual kernel functions. (a) Individual kernel functions with constant bandwidth; (b) individual kernel functions with variable bandwidth.

displayed as dashed lines. The vertical ticks on the x-axis show the locations of the data points.

The estimator given in Eq. (2) can be generalized by allowing the bandwidth to vary from data point to data point. We then obtain the sample-point adaptive estimator (e.g. Silverman, 1986)

$$\hat{f}(x) = \frac{1}{n}\sum_{i=1}^{n} \phi_{b_i}(x - X_i). \tag{3}$$

This differs from Eq. (2) in that the kernel is assumed to be normal, and that the fixed bandwidth h has been replaced data point specific bandwidths b_i (i=1,K,n) The effect of this change is illustrated in Fig. 2b, where the middle two data points have much smaller bandwidths, and hence narrow kernels, than the outer two bandwidths. Let us denote the measurement standard deviations for X_i, by σ_i, (i=1,. . .,n), so that the density of X_i is $g(x|\sigma_i)$ when σ_i is regarded as fixed. With this additional notation, we may compute the expected value of $\hat{f}(x)$:

$$\begin{aligned} E[\hat{f}(x)] &= \frac{1}{n}\sum_{i=1}^{n}\int \phi_{b_i}(x-y)g(y|\sigma_i)\mathrm{d}y \qquad (4)\\ &= \frac{1}{n}\sum_{i=1}^{n}\int \phi_{b_i}(x-y)f*\phi_{\sigma_i}(y)\mathrm{d}y \\ &= \frac{1}{n}\sum_{i=1}^{n}\int\int \phi_{b_i}(x-y)f(z)\phi_{\sigma_i}(y-z)\mathrm{d}z\mathrm{d}y \\ &= \frac{1}{n}\sum_{i=1}^{n}\int f(z-x)\phi_{b_i}*\phi_{\sigma_i}(z)\mathrm{d}z \\ &= \frac{1}{n}\sum_{i=1}^{n} f*\phi_{k_i}(x) \end{aligned}$$

where $k_i = \sqrt{b_i^2 + \sigma_i^2}$. In deriving this expression, we have used the fact that the convolution of two normal

densities, each with zero mean and with standard deviations b_i and σ_i, is itself a normal density with mean zero and standard deviation k_i. See Wand and Jones (1995, Appendix C) for an example.

Now, suppose that we chose the sample point bandwidth in Eq. (3) by $b_i = \sqrt{c^2 - \sigma_i^2}$. Then $k_i = \sqrt{c^2 - \sigma_i^2 + \sigma_i^2} = c$, and we obtain $E[\hat{f}(x)] = f^* \phi_c(x)$ from Eq. (4) so long as $c > \max\{\sigma_1, \ldots, \sigma_n\}$. We have therefore demonstrated that we can construct an estimator $\hat{f}$ whose expected value does not depend on the measurement standard deviations. However, what we are estimating is not the true age density f, but rather the transformed version of the density, or 'density functional', $f^* \phi_c$. We shall therefore refer to $\hat{f}$ as the *functional estimator* henceforth. Return to the example in the opening paragraph of this section, suppose that we choose c=38 (Ma). Then the functionals that $\hat{f}$ is estimating at sites 1 and 2 are displayed in (Fig. 3c and d), respectively. Unlike the observed age densities in Fig. 1, the density functionals are different for sites 1 and 2, displaying the same type of qualitative difference between the sites as for the true age densities. Admittedly, the functionals do not differentiate between the sites quite as clearly as the true age densities, but that is simply a reflection of the statistical difficulties in appropriately accounting for measurement error.

The discussion in the previous paragraph indicates that we can compare age distributions from different

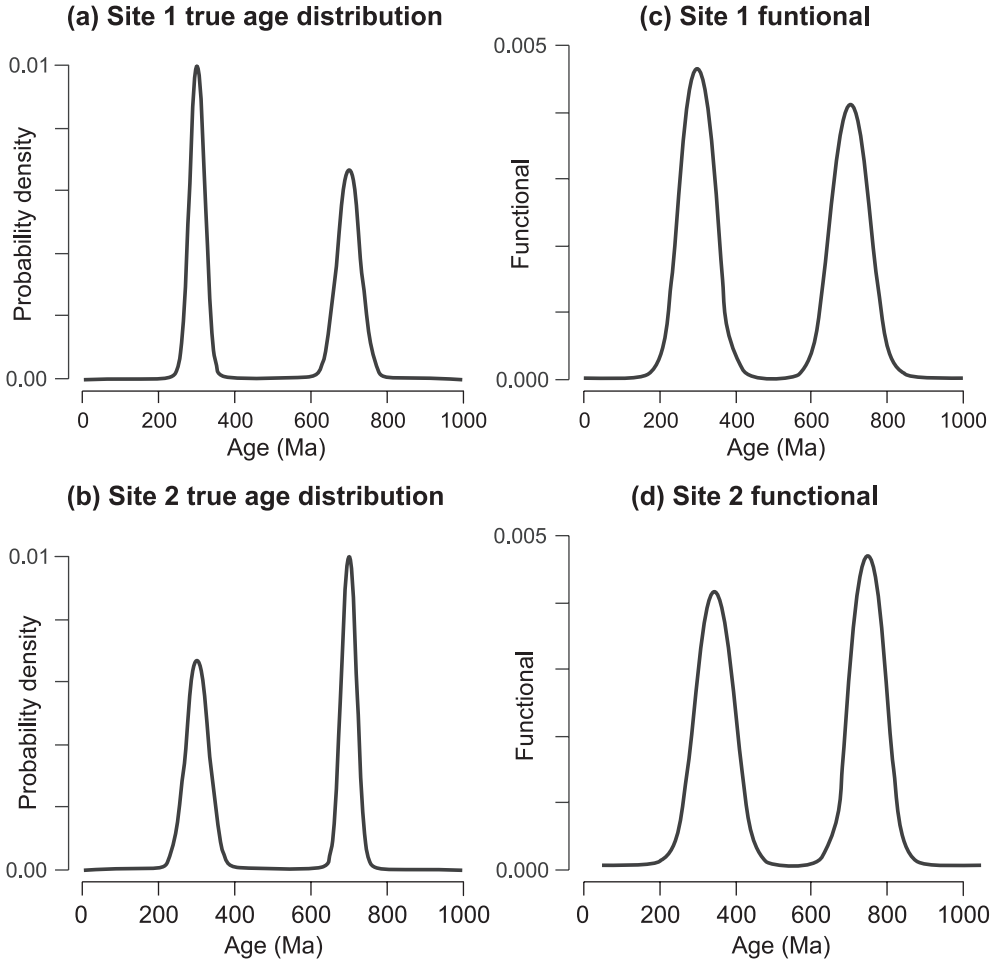

Fig. 3. (a, b) Density functions for true age distributions and (c, d) for corresponding density functionals, for two sites.

sites by comparing estimates of the corresponding density functionals. To elaborate on this, we extend our previous notation as follows. Let $X_{11},\ldots,X_{1n_1}$ be observed ages from site 1, with corresponding measurement standard deviations $\sigma_{11},\ldots,\sigma_{1n_1}$, and let $X_{21},\ldots,X_{2n_2}$ be observed ages from site 2, with corresponding measurement error standard deviations $\sigma_{21},\ldots,\sigma_{2n_2}$. As above, we assume that $X_{11},\ldots,X_{1n_1}$ and $X_{21},\ldots,X_{2n_2}$ can be regarded as random samples from the underlying distributions at sites 1 and 2, respectively. Then the age distributions between the two sites can then be compared using the following algorithm:

(1) Select $c>\max\{\sigma_{11},\ldots,\sigma_{1n_1},\sigma_{21},\ldots,\sigma_{2n_2}\}$.
(2) Construct functional estimators $\hat{f}_1$ and $\hat{f}_2$ (from Eq. (3)) from data from the first and second sites, respectively. The same value of c is used in both cases.
(3) Compute a distance between $\hat{f}_1$ and $\hat{f}_2$.

Two issues remain in order to implement this algorithm. First, how should c be chosen; second, how should the distance between $\hat{f}_1$ and $\hat{f}_2$ be calculated?

The constant c should be sufficiently large so that the smallest bandwidth, $b_{\min}$, is not too tiny. If this bandwidth is too small, then the functional estimate will be undersmoothed and have an unnatural spike at the datum corresponding to this bandwidth. On the other hand, the larger the value of c, the greater the extent to which fine detail in f will be obscured in the convolution $f*\phi_c$. This is illustrated in Fig. 4, which displays functional

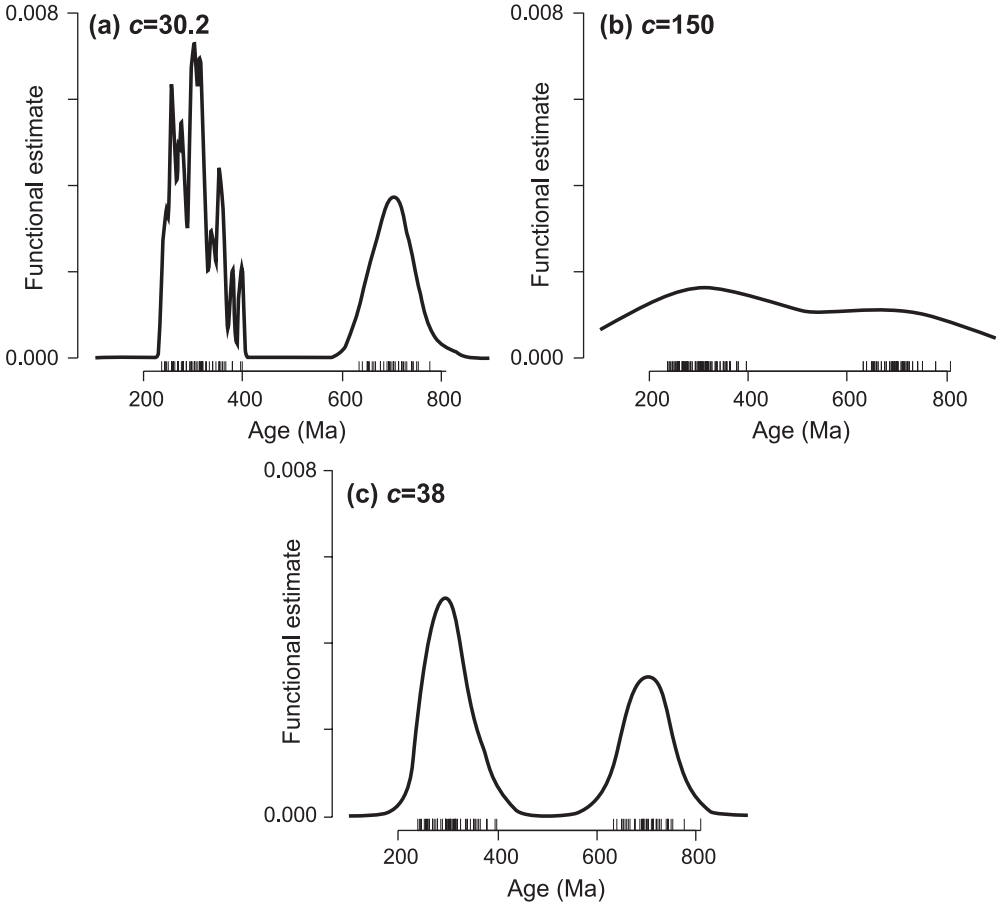

Fig. 4. Estimated functionals from data from site 1, with varying choice of smoothing parameter c.

estimates obtained from a sample of 100 ages observed at site 1 from our ongoing example. Fig. 4a depicts the functional estimate with the small value c=30.2, producing the kind of undersmoothing mentioned above. Fig. 4b shows the functional estimate with the large value c=150.0, leading to oversmoothing in which the bimodal nature of the distribution is almost obscured. An ad hoc solution is to choose

$$c = \sqrt{\sigma_{\max}^2 + h_0^2} \tag{5}$$

where $\sigma_{\max}=\max\{\sigma_{11},\ldots,\sigma_{1n_1},\sigma_{21},\ldots,\sigma_{2n_2}\}$ and $h_0=\max\{h_1,h_2\}$. Here h_i is the 'least squares cross-validation' bandwidth (Wand and Jones, 1995, Section 3.3) computed from the data observed at site i (i=1,2). The rationale for this choice is that h_1 and h_2 are relatively simple and well understood choices of bandwidth in the standard kernel density estimation problem (Silverman, 1986). With c defined according to Eq. (5), a bandwidth at least as large as h_0 will be applied at all data points, and hence there should be no undersmoothing. Applying this methodology to the data from sites 1 and 2 gave h_0=23.3 and hence c=38.0. The result functional estimate is displayed in Fig. 4c.

We now turn to quantification of the dissimilarity between $\hat{f}_1$ and $\hat{f}_2$. A natural choice is to use L_2 distance:

$$d_{12} = d(\hat{f}_1,\hat{f}_2) = \sqrt{\int \left(\hat{f}_1(x) - \hat{f}_2(x)\right)^2 \mathrm{d}x}. \tag{6}$$

The use of normal kernel functions allows this distance be expressed in closed form. More specifically, the squared distance is given by

$$\begin{aligned} d_{12}^2 = {} & \frac{1}{n_1^2}\sum_{i=1}^{n_1}\sum_{j=1}^{n_1}\phi_{\beta_{1ij}}(X_{1i}-X_{1j}) \\ & + \frac{1}{n_2^2}\sum_{i=1}^{n_2}\sum_{j=1}^{n_2}\phi_{\beta_{2ij}}(X_{2i}-X_{2j}) \\ & - \frac{2}{n_1 n_2}\sum_{i=1}^{n_1}\sum_{j=1}^{n_2}\phi_{\beta_{3ij}}(X_{1i}-X_{2j}) \end{aligned}$$

where $\beta_{1ij}=\sqrt{b_{1i}^2+b_{1j}^2}$, $\beta_{2ij}=\sqrt{b_{2i}^2+b_{2j}^2}$ and $\beta_{3ij}=\sqrt{b_{1i}^2+b_{2j}^2}$ in which b_{1i} and b_{2i} are the ith bandwidth for the first and second samples, respectively. We remark that this distance measure is dependent upon the choice of c. Hence, given three functional estimates, $\hat{f}_1$, $\hat{f}_2$ and $\hat{f}_3$, the result $d(\hat{f}_1,\hat{f}_2)<d(\hat{f}_1,\hat{f}_3)$ may be interpreted as indicating greater similarity between age distributions 1 and 2 than between age distributions 1 and 3 only if the same value of c was employed in all three cases. Furthermore, there is no absolute scale for interpreting a single distance in isolation. Instead, we must employ the machinery of statistical significance testing to determine whether an observed distance d_{12} provides evidence of a difference between the age distributions in question. We describe such a test in the following section.

In summary, the functional estimation allows comparison between sets of age data with variable measurement error by pretending that all ages have a measurement error larger than any actual measurement—the c parameter. Comparing these "smoothed" distributions avoids bias possible when attempting to compare data from different measurement techniques with varying measurement precision. An analogy can be made with the concept of upward continuation of geophysical data when attempting to combine high and low resolution data (e.g. Kearey and Brooks, 1991). The difference between two age distributions is measured as the integral of the squared difference of the two graphs when plotted on the same scale.

4. A Monte Carlo permutation test

Suppose that we observe n_1 randomly selected (error prone) ages from site 1, and n_2 randomly selected (error prone) ages from site 2. It is possible to test formally the hypothesis H_0: $f_1=f_2$ (i.e. the true age distributions are the same) against the alternative H_1: $f_1\neq f_2$ (i.e. the true age distributions are the different) using a Monte Carlo permutation test (e.g. Edgington, 1987). The idea is as follows. Suppose that the data from both sites are combined and n_1 observations are drawn at random (and without replacement) from the pooled data set, leaving n_2 data unselected. If H_0 is correct, then all the data can be regarded as

coming from one population, and hence the data sets of size n_1 and n_2 created in this fashion (the 'resampled' data) should have equivalent statistical properties to those of the original data sets. More specifically, the value of $d(\hat{f}_1,\hat{f}_2)$ obtained from the original samples should be comparable to the value of $d(\hat{f}_1^*,\hat{f}_2^*)$ where $\hat{f}_1^*$ and $\hat{f}_2^*$ are functional estimates obtained from resampled data sets. This reasoning motivates the following Monte Carlo algorithm.

4.1. Monte Carlo permutation test algorithm

(1) Compute $d_{12}=d(\hat{f}_1,\hat{f}_2)$ from the observed data.
(2) Let N denote the number of resampled data sets that we will generate. For $i=1,\ldots,N$:
   (i) Pool all of the observed data. Randomly sample (without replacement) n_1 observations from the pooled data with corresponding measurement error standard deviations. Denote this data set by $X_{11}^*,\ldots,X_{1n_1}^*$ and denote the corresponding measurement error standard deviations by $\sigma_{11}^*,\ldots,\sigma_{1n_1}^*$. Denote the remaining set of n_2 data points and their corresponding measurement error standard deviations by $X_{21}^*,\ldots,X_{2n_2}^*$ and $\sigma_{21}^*,\ldots,\sigma_{2n_2}^*$, respectively.
   (ii) Construct functional estimate $\hat{f}_1^*$ from $X_{11}^*,\ldots,X_{1n_1}^*$ and $\sigma_{11}^*,\ldots,\sigma_{1n_1}^*$, and construct $\hat{f}_2^*$ from $X_{21}^*,\ldots,X_{2n_2}^*$ and $\sigma_{21}^*,\ldots,\sigma_{2n_2}^*$.
   (iii) Compute $d_{12}^*[i]=d(\hat{f}_1^*,\hat{f}_2^*)$.
(3) Compute test P-value by $P=(1/N)\sum_{i=1}^{N} I\left(d_{12}<d_{12}^*[i]\right)$ where I is the indicator variable defined for any event A by $I(A)=1$ if A occurs and 0 otherwise. Note that P is simply the proportion of the Monte Carlo distances $d_{12}^*[1],\ldots,d_{12}^*[N]$ that are greater than the distance computed from the original observed data.

The number of Monte Carlo samples, N, should be chosen so as to balance the competing requirements of precision in the P-value and computational speed. A value of 1000 would be a suitable choice in general.

5. Clustering and dendrograms

A computed array of similarity or distance measurements also provides the basis for clustering methods that illustrate relationships among samples. Such clustering methods are a common aspect of fields such as taxonomy dealing with sample classification (e.g. Sneath and Sokal, 1973; Gordon, 1999). Hierarchical (or agglomerative) clustering methods are most widely used in geological applications and can produce tree-like dendrograms that summarize sample similarity (e.g. Davis, 1986, p. 503; Burrett and Berry, 2002; Swan and Sandilands, 1995).

Hierarchical clustering begins by pairing the two samples with the least distance (=greatest similarity). This pair is then treated as a single sample and the distance array is recalculated accordingly. The next two samples with the least distance are then clustered and the array recalculated. The process continues until all samples have been merged.

There are a variety of methods for assessing the least distance between clusters (Sneath and Sokal, 1973; Hartigan, 1975; Davis, 1986; Swan and Sandilands, 1995; Gordon, 1999). For instance, two samples or clusters may be merged because the average distance between all members of those clusters is the least. The array is then recalculated to measure the average distance between all remaining clusters. Other methods use single (or complete) linkages where the least distance (or even the greatest distance) between any two members in two clusters is the clustering criteria.

An unweighted average clustering method has been used here for the sake of simplicity although there is no simple solution to judge which clustering method is best. It should be emphasized that this stage introduces an element of subjectivity back into the interpretative process. Swan and Sandilands, (1995, p. 396) discuss this further and suggest that although clustering is generally useful for illustrating structures within data, profound conclusions should not be made.

Davis (1986, p. 513) suggests the use of a cophenetic values to assess any distortion in the clustering process. The cophenetic distance is the distance that two samples actually merge during

the clustering process. The cophenetic correlation coefficient is calculated as the correlation between the original distance between all the samples and the cophenetic distance. The greater the correlation the less the merging has distorted the samples from their original distances. It is recommended that regardless of the clustering method chosen the cophenetic correlation coefficient is reported.

Finally, regardless of the clustering method chosen, a dendrogram graphically illustrates when samples (represented by branches) merge at the levels of similarity calculated in the clustering process. The further along the distance coefficient axis two samples (or the clusters they are part of) merge the more dissimilar they are. Drawing a phenon line (Swan and Sandilands, 1995) across the dendrogram at an arbitrary distance level where numerous samples have been amalgamated to fewer clusters may emphasise those clusters as having some inherent significance and aid interpretation of the data. However, because the phenon line distance is arbitrary, it is a qualitative classification method and should only be used for illustrative purposes. An example of a dendrogram and how it can used to illustrate the relationships in a large set of age data is given in Section 6.4.

6. Examples

6.1. Synthetic example data: unimodal components

Seven sets of unimodal data were synthetically generated to illustrate the quantification of comparison between different modes of age data. Each set consisted of 100 ages and measurement uncertainty that yield normal distributions based around a mean value (100, 101, 105, 110, 125, 1000 and 4000 Ma) with a standard deviation of 5 My. The measurement error standard deviation is 10 My. The calculated distances between age functional estimates are given in Table 1 and each is computed using the same value of c (15.7) to ensure comparability. The P-values for Monte Carlo permutation test of equal true distributions are also presented in this table.

As expected, the distances increase as the mean of the age distributions become increasingly displaced. Tests for equality of distributions provides statistically significant evidence (at a 5% level) of differences between all pairs of distributions except for the T1–T2, T2–T3 and comparisons. These two positive results indicate the methodological limits in resolving close age components.

6.2. Synthetic example data: modal precision

Six sets of unimodal data were synthetically generated to illustrate the quantification of comparison between unimodal age data of varying degrees of measurement uncertainty. Each set consisted of 100 ages where the true age distribution was normal with mean 1000 Ma and standard deviation 5 My in all six cases. The measurement error standard deviations were 1, 2, 5, 10, 20 and 50 My, respectively. The calculated distances between age functional estimates and the P-values for Monte Carlo permutation test of equal true distributions are given in Table 2. Again, a

Table 1
Matrix of comparison between the seven synthetic data sets drawn from age distributions, T1–T7, with varying mean

	T1	T2	T3	T4	T5	T6	T7
T1: $N(100,5)\pm10$		*0.219*	*0.002*	*0*	*0*	*0*	*0*
T2: $N(101,5)\pm10$	**7.4**		*0.053*	*0*	*0*	*0*	*0*
T3: $N(105,5)\pm10$	24.4	18.1		*0.066*	*0*	*0*	*0*
T4: $N(110,5)\pm10$	41.3	35.9	18.6		*0*	*0*	*0*
T5: $N(125,5)\pm10$	104.4	100.5	84.1	65.9		*0*	*0*
T6: $N(1000,5)\pm10$	171.2	171.9	170.2	168.7	174.0		*0*
T7: $N(4000,5)\pm10$	173.0	173.7	172.0	170.6	**175.8**	173.0	

These distributions are described in the left-hand column, where the notation $N(\alpha,\beta)\pm\gamma$ indicates that the age distribution is normally distributed with mean α and standard deviation β, and the measurement error standard deviation is γ. The value of c for this comparison was 15.7. The values in the lower left half of the table are the calculated distances between the functional estimates, multiplied by 10^3. The bold values are the minimum and maximum values. The italicized values in the upper right half are P-values for testing equality of age distributions.

Table 2
Matrix of comparison between the seven synthetic data sets drawn from age distributions, U1–U6, with varying degrees of measurement error

	U1	U2	U3	U4	U5	U6
U1: $N(1000,5)\pm1$		*0.192*	*0.297*	*0.442*	*0.894*	*0.412*
U2: $N(1000,5)\pm2$	**0.1**		*0.323*	*0.595*	*0.765*	*0.279*
U3: $N(1000,5)\pm5$	0.2	0.3		*0.330*	*0.791*	*0.322*
U4: $N(1000,5)\pm10$	0.7	0.6	0.8		*0.467*	*0.219*
U5: $N(1000,5)\pm20$	1.2	1.2	1.0	1.0		*0.210*
U6: $N(1000,5)\pm50$	**12.1**	12.0	11.9	11.8	10.9	

These distributions are described in the left-hand column, where the notation $N(\alpha,\beta)\pm\gamma$ indicates that the true age distribution is normally distributed with mean α and standard deviation β, and that the measurement error standard deviation is γ. The values in the lower left half of the table are the calculated distances between the functional estimates, multiplied by 10^3. The value of c for this comparison was 78.6. The italicized values in the upper right half are P-values for testing equality of age distributions.

common value of c (78.6) was used to ensure comparability. This differs from the value of c employed in the previous example and emphasises that comparisons between age data are dependent on the actual data being analysed; i.e. attempting to compare the results in Tables 1 and 2 is meaningless without repeating the calculations on all the samples at the same time.

While the calculated distance between estimates increases by a modest amount as the measurement error becomes more pronounced, none of the permutation tests provide significant evidence against the hypothesis of equal underlying true age distributions (i.e. all P-values greater than 0.05 in Table 2). This indicates that there is no significant bias in the results of comparison between functional estimates based on high and low precision data. Therefore this methodology should be applicable to a wide range of age dating techniques provided that the samples selected are representative of the complete population.

6.3. Application: Ovens Graben, New South Wales

Exotic Neoproterozoic-aged zircon grains are a common feature of sedimentary rocks in southeastern Australia (Ireland et al., 1998; Sircombe, 1999; Veevers, 2000), but the provenance of these grains is enigmatic. The Mid-Triassic Hawkesbury Sandstone of the Sydney Basin, New South Wales, is a significant part of this problem because it represents an influx of southwesterly derived cratonic detritus with a dominant exotic Neoproterozoic detrital zircon age distribution into a foreland basin setting otherwise dominated by Palaeozoic material from the northeast. The mystery is further compounded by the paucity of zircon ages in the Hawkesbury Sandstone that can be attributed to the Palaeozoic Lachlan Fold Belt even though the Mid-Triassic fluvial system flowed over this geological region.

Southwest of the Sydney Basin, the Ovens Graben is an infrabasin beneath the Cainozoic Murray Basin and is considered to contain sedimentary units deposited coevally with the Hawkesbury Sandstone (Veevers, 1984, p. 241). Because a confirmed correlation would provide further information about the provenance and palaeogeography of the Hawkesbury Sandstone, three Permian–Triassic samples from the Ovens Graben, in particular the Jerilderie Formation, have been examined to search for potential correlations with previously examined Sydney Basin samples.

Detrital zircon grains were extracted from drill core using standard methods. Isotopic dating was made by an excimer laser ablation-inductively coupled plasma-mass spectrometer (ELA-ICP-MS) at the Research School of Earth Sciences, Australian National University, based on procedures modified from Horn et al. (2000) and further described in Appendix B.

The results of functional estimation and permutation testing of these data against previously examined eastern Australian samples in the Sydney and Murray Basin (Sircombe, 1999) are given in Table 3 and illustrated in Fig. 5. This data set also provides an opportunity to examine the response of the technique to age data from different techniques resulting in different measurement errors. Previous eastern Australian zircon samples were analysed by SHRIMP whereas the Ovens Graben samples were analysed by ELA-ICPMS and have a greater precision (Fig. 5).

The calculated P-values (Table 3; Fig. 5) indicate that the null hypothesis of equal age distributions between Urana, Jerilderie-A and Jerilderie-B samples cannot be rejected at a 5% significance level. Beyond Ovens Graben, there are no grounds for rejecting equality between the Urana and Tallong, Spring Hill and WIM-150 samples. A similar conclusion exists between the Jerilderie-B and Tallong samples at 5%

Table 3
Matrix of comparison between the zircon age data for Ovens Graben, Murray Basin and Sydney Basin

	c=159	CAL	BUN	TER	TAL	SPR	HIS	ROB	WIM	JRA	JRB	URA
Sydney Basin	CAL: Calga		*0.236*	*0*	*0*	*0*	*0*	*0.007*	*0*	*0*	*0*	*0*
	BUN: Bundeena	5.89		*0*	*0*	*0*	*0*	*0.007*	*0*	*0*	*0*	*0*
	TER: Terrigal	28.89	***29.42***		*0*	*0*	*0*	*0*	*0*	*0*	*0*	*0*
	TAL: Tallong	19.62	21.40	12.51		*0*	*0*	*0*	*0.869*	*0*	*0.183*	*0.806*
Murray Basin	SPR: Springhill	15.66	15.08	16.44	13.80		*0.314*	*0.016*	*0.001*	*0*	*0*	*0.027*
	HIS: Hispanola	20.47	18.80	15.96	17.12	6.23		*0*	*0*	*0*	*0*	*0*
	ROB: Robinvale	11.06	14.06	22.48	14.86	11.46	16.54		*0*	*0*	*0*	*0*
	WIM: WIM-150	18.77	20.31	12.23	***2.86***	12.28	15.55	14.33		*0*	*0.043*	*0.723*
Ovens Graben	JRA: Jerilderie-A	15.16	18.02	18.83	7.22	14.77	19.58	11.97	7.38		*0.135*	*0.036*
	JRB: Jerilderie-B	17.09	19.40	15.94	5.53	13.97	17.80	13.51	4.83	5.08		*0.388*
	URA: Urana	15.98	17.13	14.69	4.76	10.93	14.63	12.85	4.19	7.26	6.01	

The value of c for this comparison is 159. The values in the lower left half are the calculated distances between the age distribution estimations multiplied by 10^3 shaded from white (smaller d) to dark grey (larger d). Bold numbers indicate the maximum and minimum distance values. The italicized values in the upper right half are P-values for testing equality of age distributions. Dark shaded cells have $P<0.01$, medium shaded cells have $0.05>P>0.01$, unshaded cells have $P>0.05$.

significance although Jerilderie-A has no significant relationship with any sample outside the Ovens Graben. Importantly, the permutation testing between the Jerilderie Formation and Hawkesbury Sandstone Formation samples (Calga and Bundeena) indicate that equality can be rejected.

Because the Tallong Conglomerate and WIM-150 samples are strongly associated with a Lachlan Fold Belt provenance (Sircombe, 1999), at least the Urana sample is interpreted as having a similar provenance. The same conclusion is drawn for the Jerilderie samples, although apparently weaker correlation suggests that the age components present may be somewhat different from those seen in the other Lachlan Fold Belt derived samples examined in this analysis.

These results quantify the interpretation of the Ovens Graben sedimentary rocks as being derived from the nearby Palaeozoic–Mesozoic basement rather than linked with an exotic Neoproterozoic provenance. Therefore, while there are striking stratigraphic and lithologic similarities between the Jerilderie Formation and Hawkesbury Sandstone these are not seen in the corresponding detrital zircon age distributions. This result further constrains interpretation of the palaeogeography of the Hawkesbury Sandstone and suggests that fluvial transportation of detritus across southeastern Australia may have been quite restricted.

6.4. Application: Neoproterozoic and Cambrian sandstones, Australia–Tasmania

Berry et al. (2001) examined five Neoproterozoic and Cambrian sandstones in Tasmania to examine potential correlation with mainland Australia in comparison with previously measured detrital zircon age distributions from elsewhere in Tasmania (Black et al., 1997) the Adelaide and Lachlan foldbelts (Ireland et al., 1998). This comparison has been expanded here to include detrital zircon geochronology from Amadeus Basin (Camacho et al., 2002). Unfortunately, the comparison with qualitatively chosen zircon data from Nevada used by Berry et al. (2001) is not statistically valid using the method described here.

The results quantify the similarity between these 25 detrital zircon samples and thus the interpretation of tectonic significance of these similarities (Table 4). Clustering was performed with an averaging algorithm and the cophentic correlation coefficient was 0.82. The dendrogram (Fig. 6) can be cut at a distance level of 12.5 to define four distinct clusters.

The first cluster consists of samples dominated by modes in the 1500–2000 Ma age range and also contains representatives from all regions except the Amadeus and Kanmantoo, but is particularly dominated by Tasmanian Neoproterozic samples. The

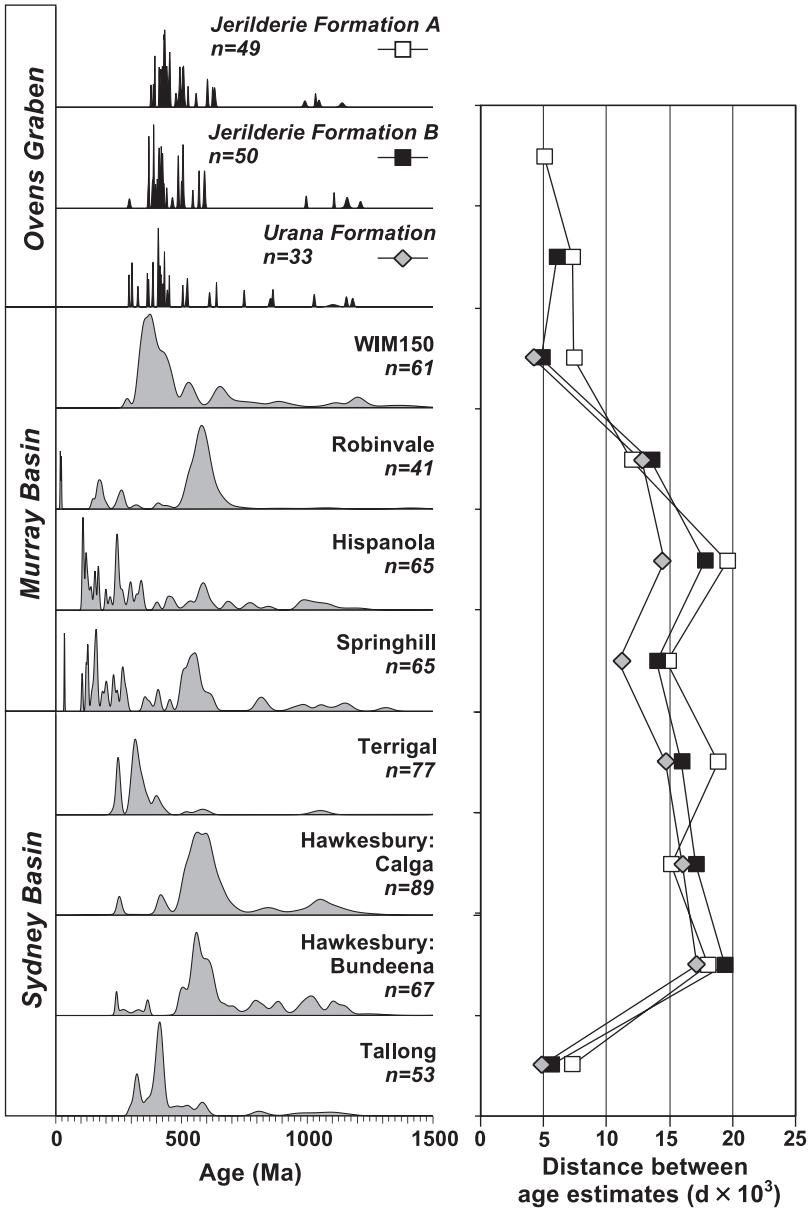

Fig. 5. Comparison of detrital zircon age distributions from Ovens Graben with Murray Basin and Sydney Basin samples as described in text. Left-hand column is age distribution plots summing individual Gaussian distributions (Sircombe, 2004). The vertical axis on these plots represents probability density with the vertical scale altered for clarity; *n* indicates the number of individual age measurements in each distribution. The spikiness of the distributions for the three Ovens Graben samples at top illustrates the precision difference between these ELA-ICPMS analyses and the remaining SHRIMP analyses. Right-hand column illustrates the distance between age estimates for the Ovens Graben samples. Hollow squares: Jerilderie-A; filled squares: Jerilderie-B; grey-filled diamonds: Urana.

Table 4
Matrix of comparison between the detrital zircon age data from Neoproterozoic and Cambrian sedimentary strata in Tasmania, southeastern and central Australia

	c=240	SQ	AC	SR	GG	FC	DTN	JCB	OON	TYN	NEE	KOS	BAL	FLE	CAR	HEA	MTF	BON	MAR	MIT	NIG	MTC	AYR	WIN	INU	INL
Tasmania Cambrian	SQ: Stitt Quartzite (1)		*0.150*	*0.055*	*0.282*	*0.135*	*0.149*	0	*0.753*	*0.007*	*0.130*	0	0	0	0	0	*0.003*	*0.003*	0	*0.014*	*0.295*	0	0	0	0	0
	AC: Animal Creek Gwke (1)	8.24		*0.002*	*0.851*	0	*0.009*	*0.022*	*0.069*	0	0	0	0	0	0	0	0	*0.112*	*0.001*	*0.091*	*0.001*	0	0	0	*0.006*	0
	SR: Sticht Range Fm. (1)	7.31	14.61		*0.012*	*0.004*	*0.001*	0	*0.181*	*0.007*	0	0	0	0	0	0	*0.041*	0	0	0	0	0	0	0	0	0
	GG: Gog Gwke. (1)	6.99	4.00	13.28		*0.001*	*0.239*	*0.037*	*0.333*	*0.016*	*0.043*	0	0	0	0	0	*0.001*	*0.109*	*0.008*	*0.296*	*0.122*	0	0	0	*0.021*	0
Tasmania Neoprot.	FC: Forest Cnglm. (1)	5.35	11.53	5.67	9.55		*0.192*	0	*0.040*	*0.116*	*0.381*	0	0	0	0	0	0	0	0	0	*0.044*	0	0	0	0	0
	DTN: Detention Subgrp. (2)	5.79	9.16	9.29	7.10	3.92		0	0	0	*0.300*	0	0	0	0	0	0	0	0	0	0	0	0	0	0	0
	JCB: Jacob Quartzite (2)	15.68	9.00	21.78	9.14	18.35	15.64		0	0	0	0	0	0	0	0	0	*0.030*	*0.175*	*0.009*	0	0	0	0	*0.118*	0
	OON: Oonah Frm. (2)	3.58	9.07	7.38	8.68	5.56	5.87	17.38		0	0	0	0	0	0	0	0	0	0	0	0	0	0	0	0	0
	TYN: Tyennan Element (2)	7.63	13.99	4.45	12.22	2.92	6.45	20.86	7.25		*0.001*	0	0	0	0	0	0	0	0	0	0	0	0	0	0	0
	NEE: Needles Quartzite (2)	5.18	10.22	7.58	8.08	2.05	***2.01***	16.84	5.53	4.78		0	0	0	0	0	0	0	0	0	*0.004*	0	0	0	0	0
Lachlan F.B.	KOS: Mt. Kosciusko (3)	29.45	22.67	34.31	25.45	32.56	30.76	21.24	30.05	34.45	31.56		*0.093*	*0.598*	*0.004*	0	0	0	0	0	0	0	0	0	0	0
Kanmantoo Group	BAL: Balquhidder Fm (3)	31.26	24.99	35.84	28.11	34.44	32.85	24.97	31.53	36.19	33.56	5.20		*0.195*	*0.291*	0	0	0	0	0	0	0	0	0	0	0
	FLE: Fleurieu Shear Zn. (3)	31.42	24.96	36.11	27.90	34.66	33.03	24.16	31.88	36.48	33.76	3.52	2.98		*0.012*	0	0	0	0	0	0	0	0	0	0	0
	CAR: Carrickalinga Hd. (3)	31.63	25.64	36.19	28.94	34.90	33.33	26.57	31.58	36.61	34.05	8.41	3.85	6.13		0	0	0	0	0	0	0	0	0	0	0
Normanville Group	HEA: Heatherdale Shale (3)	31.10	23.83	36.60	25.27	34.20	31.91	17.23	32.48	36.41	32.94	15.27	20.04	17.82	22.77		0	0	*0.001*	0	0	*0.006*	0	*0.018*	0	*0.360*
	MTF: Mt. Terrible Frm. (3)	10.39	17.08	6.72	16.72	11.37	14.33	24.82	9.81	10.68	12.92	34.71	35.61	36.00	35.51	38.12		0	0	0	0	0	0	0	0	0
Adelaide Neoprot.	BON: Bonney Sst. (3)	14.80	8.20	20.19	9.91	18.03	16.24	7.27	16.21	20.19	16.99	16.69	20.03	19.28	21.59	16.67	21.93		*0.011*	0	0	0	0	0	*0.165*	0
	MAR: Marino Arkose (3)	19.94	12.93	25.82	13.59	22.74	20.23	5.14	21.60	25.15	21.33	18.13	22.45	21.20	24.50	12.24	28.38	7.63		*0.002*	0	0	0	*0.086*	*0.676*	*0.001*
	MIT: Mitcham Quartzite (3)	10.71	5.73	16.27	4.41	12.53	10.05	6.40	12.46	14.97	11.06	23.37	26.55	26.13	27.86	22.26	20.07	7.98	10.45		*0.002*	0	0	0	*0.016*	0
	NIG: Niggly Gap Beds (3)	4.36	8.50	9.38	7.09	5.01	3.44	15.90	4.17	7.62	3.67	29.94	31.72	32.01	31.96	31.80	13.15	15.88	20.33	10.63		0	0	0	0	0
Amadeus Cambrian	MTC: Mt. Currie Congl. (4)	35.54	28.50	41.06	29.49	38.54	36.16	20.89	37.09	40.77	37.23	21.38	25.99	23.71	28.70	6.41	***42.82***	21.79	16.13	26.42	36.25		*0.003*	0	0	*0.008*
	AYR: Ayers Rock Arkose (4)	34.42	27.50	40.11	28.19	37.33	34.82	19.30	36.11	39.65	35.95	22.95	27.60	25.47	30.24	8.25	42.22	21.39	14.94	25.16	35.02	4.04		0	0	0
Amadeus Neoprot.	WIN: Winnall Beds (4)	24.66	17.36	30.67	18.62	27.92	25.38	10.38	26.02	30.31	26.55	17.15	21.57	19.94	23.59	7.88	32.41	11.57	6.13	16.07	25.21	11.49	10.80		*0.007*	*0.147*
	INU: Upper Inindia Beds (4)	18.49	11.37	24.12	12.22	21.01	18.56	5.00	20.03	23.32	19.63	17.28	21.45	20.41	23.49	13.66	26.86	5.97	2.94	8.74	18.76	18.12	17.23	8.38		0
	INL: Lower Inindia Beds (4)	28.92	21.85	34.52	23.00	32.04	29.73	14.86	30.39	34.29	30.76	16.94	21.72	19.64	24.23	3.46	36.14	14.99	9.93	20.07	29.63	7.05	7.83	5.40	11.77	

Data sources: (1) Berry et al., 2001; (2) Black et al., 1997; (3) Ireland et al., 1998; (4) Camacho et al., 2002. The values in the lower left half are the calculated distances between the age distribution estimations multiplied by 10^3 shaded from white (smaller d) to dark grey (larger d). Bold values indicate minimum and maximum. The value of c for this comparison was 240. The italicised values in the upper right half are P-values for testing equality of age distributions. Dark shaded cells have $P<0.01$, medium shaded cells have $0.05>P>0.01$, light shaded cells have $P>0.05$.

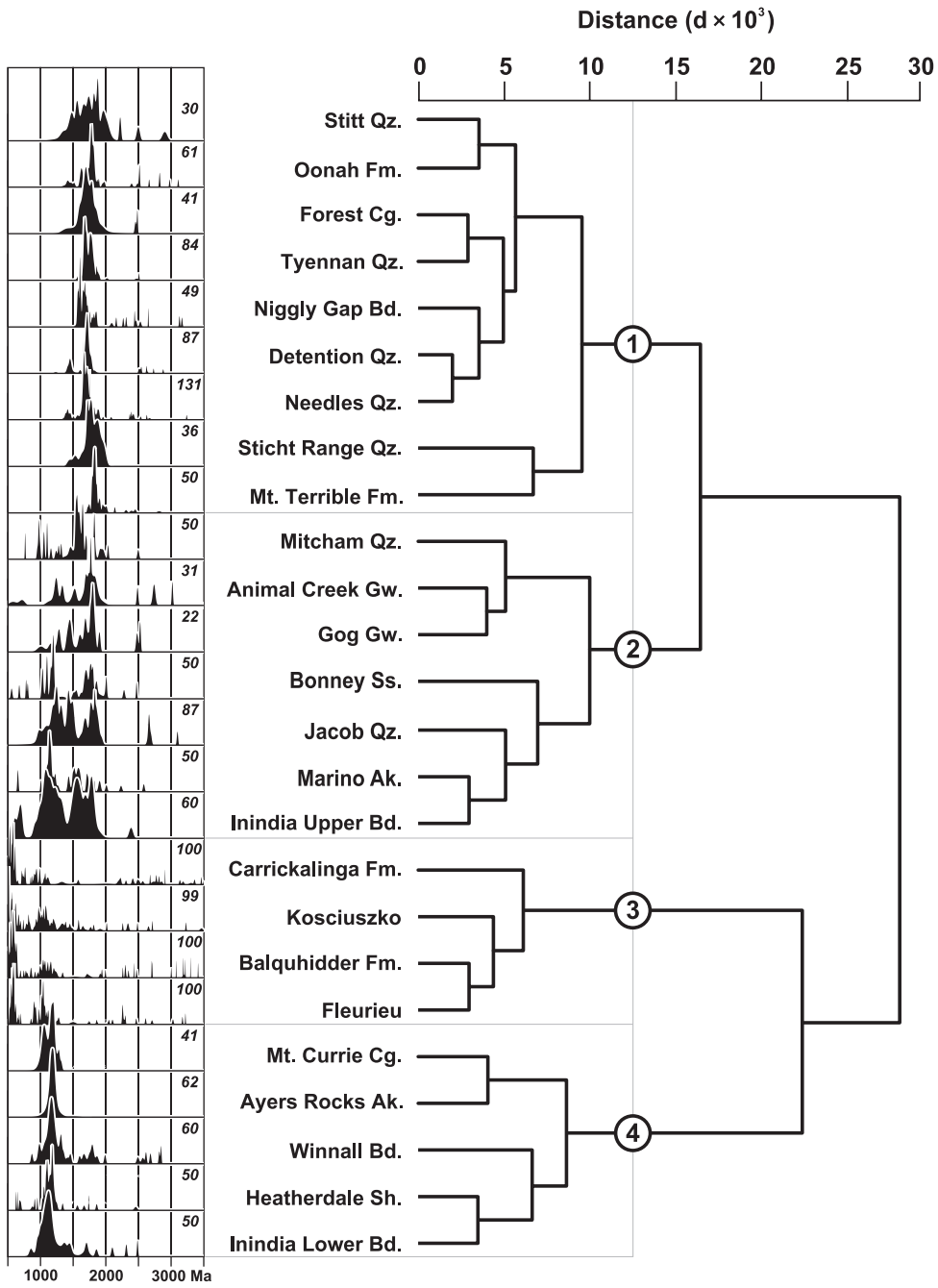

Fig. 6. Dendrogram illustrating the similarity relationships among Tasmanian, Adelaidean and Amadeus detrital zircon age data. Phenon line at distance of 12.5 creates four clusters discussed in the text. Age probability density distribution plots summing individual Gaussian distributions (Sircombe, 2004) are given in left-hand column. The vertical axis on these plots represents probability density with the vertical scale altered for clarity; the number associated with each plot indicates the number of individual age measurements in each distribution. References for data given in Table 4. Average clustering method used; cophenetic correlation: 0.82.

close similarity of two Tasmanian Cambrian samples (Sticht Range and Stitt Quartzites) with Neoproterozoic samples reinforces previous interpretations (Berry et al., 2001) that many of the Tasmanian Cambrian detrital zircons have been recycled from Neoproterozoic units.

The second cluster consists of samples that display a wide range of ages from 500 to 2500 Ma with principal modes at ~1250 and ~1750 Ma. This cluster contains representatives from the Tasmanian Cambrian and the Neoproterozoic in the Tasmanian, Adelaidean and Amadeus regions. In the Amadeus, the older component is interpreted as an Arunta Inlier or Gawler craton provenance (Camacho et al., 2002). Clustering here suggests that this source was also available for the middle and top of the Adelaidean succession (Marino Arkose, Bonney Sandstone and Mitcham Quartzite) and possibly the Neoproterozoic in Tasmania (Jacob Quartzite) with subsequent recycling into the Cambrian (Animal Creek and Gog Greywackes).

The third cluster consists of the three Cambrian Kanmantoo Group samples and Mt. Kosciuszko with age distributions generally consisting of a major component at 500–700 Ma, a minor component at 900–1200 Ma and scattering of ages into the Archean. The distinctiveness of this group is well known and is interpreted as being derived from the Neoproterozoic Ross-Delamerian orogen (Ireland et al., 1998)—a source apparently unavailable to Cambrian-aged samples in Tasmania or the Amadeus.

The fourth cluster consists largely of the Amadeus Cambrian and Neoproterozoic samples dominated by age modes in the 1000–1500 Ma age range interpreted as derived from the Musgrave Complex (Camacho et al., 2002). The inclusion of the Cambrian Heatherdale Shale from the Normanville Group within this cluster suggests that there may be some provenance links between the Musgrave Complex and younger successions within the Adelaide region.

7. Concluding remarks

The kernel functional estimation methodology presented here is an advance on other methods comparing detrital zircon age distributions. Previous methods have been inadequate in either not having an inherent statistical test or not accounting for measurement uncertainty in the data. Sample data must also quantitatively represent the age distributions—a strict criterion that may exclude a lot of existing data in the literature.

The methodology described here has been demonstrated for both synthetic and real data. While the calculated distance between age estimates increases with increased precision of the data, the probability of similarity does not fall below significance levels (Table 2). In application to real data, the results have been consistent with previous measurements of similarity as well as pointing out further subtleties in interpretation (Tables 3 and 4). Application to provenance problems with both regional and global scope has demonstrated the ability to quantify relationships between samples to aid provenance interpretations in situations with implications for tectonic and palaeogeographic reconstructions.

The principal advantage of this methodology will be in providing a quantification of similarity between detrital zircon age distributions and is thus a powerful tool in the further development of detrital zircon geochronology.

Acknowledgments

KNS supported by ARC Discovery Grant DP0208797. Valuable assistance with acquisition of ELA-ICPMS data for the Ovens Graben samples was provided by C. Allen, I. Campbell and M. Palin, Research School of Earth Sciences, Australian National University. R. Berry provided important comments on an earlier draft. A. Carter and B. Székely provided constructive reviews. TSRC contribution no. 274.

Appendix A. Implementation of algorithms

The techniques described in this paper have been applied using “R”, a system for statistical computation and graphics (Ihaka and Gentleman,

1996; Grunsky, 2002). It is free software distributed under a GNU-style system and can be accessed at http://www.r-project.org/. The functional estimation and Monte Carlo permutation testing algorithms have been implemented using the following functions:

```
#############################################################
## Density estimator with sample-point adaptive bandwidth ##
#############################################################

adapt.f <- function(x,h,eval){
f <- eval*0
for (i in 1:length(eval)){f[i] <- mean(dnorm(x-eval[i],0,sd=h))}
f}

sig2.con <- function(x,sigx,UCV=TRUE){
  sig2max <- max(sigx^2)
  h <- 1.06*min(sd(x),IQR(x)/1.34)/length(x)^0.2
  if (UCV) h <- bw.ucv(x,lower=h/20,upper=h)
  sig2.con <- sig2max+h^2
  sig2.con}

######################
## Permutation Test ##
######################

## Calculate integrated squared KDEs ##

Rf <- function(x,sig2,c.con){
  h1 <- sqrt(c(outer(c.con-sig2,c.con-sig2,"+")))
  xdiff <- c(outer(x,x,"-"))
  rf <- mean(dnorm(xdiff,sd=h1))
  rf}

## L2 distance between KDEs ##

dXY <- function(x,sig2x,y,sig2y,c.con=0){
  if (c.con <= 0) c.con <- max(sig2.con(x,sigx),sig2.con(y,sigy))
  rfx <- Rf(x,sig2x,c.con)
  rfy <- Rf(y,sig2y,c.con)
  h1 <- sqrt(c(outer(c.con-sig2x,c.con-sig2y,"+")))
  XYdiff <- c(outer(x,y,"-"))
  Itmp <- mean(dnorm(XYdiff,sd=h1))
  dxy <- rfx+rfy-2*Itmp
  dxy <- sqrt(dxy)
}

## Permutation Test for Equality of KDEs ##

Perm.Test <- function(x,y,sigx,sigy,c.con=0,REP=1000){
nx <- length(x)
ny <- length(y)
n <- nx+ny
xandy <- c(x,y)
allsig <- c(sigx,sigy)
if (c.con <= 0) c.con <- max(sig2.con(x,sigx),sig2.con(y,sigy))
dxy <- dXY(x,sigx^2,y,sigy^2,c.con)
P <- 0

for( i in 1:REP ){
  perm.index <- sample(1:n)
  x.index <- perm.index[1:nx]
  y.index <- perm.index[(nx+1):n]
  X <- xandy[x.index]
  Y <- xandy[y.index]
  sigX <- allsig[x.index]
  sigY <- allsig[y.index]
  dxy.2 <- dXY(X,sigX^2,Y,sigY^2,max(sig2.con(X,sigX),sig2.con(Y,sigY)))
  P <- P + (dxy.2 > dxy)
        }
P <- P/REP
P}
```

Age data (age and 1 sigma measurement uncertainty) are loaded from comma delimited text files (CSV). A typical analytical session in R, using the Tasmanian data of Berry et al. (2001) as an example, would be as follows:

```
source("rcode3.txt") # access implemented algorithms

# read in data from csv text files
SQ <- read.csv('SQ.csv')
attach (SQ)
AC <- read.csv('AC.csv')
attach (AC)
SR <- read.csv('SR.csv')
attach (SR)
GG <- read.csv('GG.csv')
attach (GG)
FC <- read.csv('FC.csv')
attach (FC)

# calculate 'c' value for data (this returns c^2)
Run.c2 <- max(sig2.con(SQ.x,SQ.sd),
sig2.con(AC.x,AC.sd),sig2.con(SR.x,SR.sd),
sig2.con(GG.x,GG.sd),sig2.con(FC.x,FC.sd))

# set up array for results
results <- array(0,c( 5, 5))
colnames(results) <- c("SQ","AC","SR","GG","FC")
rownames(results) <- c("SQ","AC","SR","GG","FC")

# place c value in first cell of array for later reference
results[1,1] <- Run.c2

# calculate distances
results[ 2, 1] <- (dXY(SQ.x,SQ.sd,AC.x,AC.sd,c.con=Run.c2))*1000
results[ 3, 1] <- (dXY(SQ.x,SQ.sd,SR.x,SR.sd,c.con=Run.c2))*1000
results[ 4, 1] <- (dXY(SQ.x,SQ.sd,GG.x,GG.sd,c.con=Run.c2))*1000
results[ 5, 1] <- (dXY(SQ.x,SQ.sd,FC.x,FC.sd,c.con=Run.c2))*1000
results[ 3, 2] <- (dXY(AC.x,AC.sd,SR.x,SR.sd,c.con=Run.c2))*1000
results[ 4, 2] <- (dXY(AC.x,AC.sd,GG.x,GG.sd,c.con=Run.c2))*1000
results[ 5, 2] <- (dXY(AC.x,AC.sd,FC.x,FC.sd,c.con=Run.c2))*1000
results[ 4, 3] <- (dXY(SR.x,SR.sd,GG.x,GG.sd,c.con=Run.c2))*1000
results[ 5, 3] <- (dXY(SR.x,SR.sd,FC.x,FC.sd,c.con=Run.c2))*1000
results[ 5, 4] <- (dXY(GG.x,GG.sd,FC.x,FC.sd,c.con=Run.c2))*1000
# calculate test of equality values
results[ 1, 2] <- Perm.Test(SQ.x,AC.x,SQ.sd,AC.sd)
results[ 1, 3] <- Perm.Test(SQ.x,SR.x,SQ.sd,SR.sd)
results[ 1, 4] <- Perm.Test(SQ.x,GG.x,SQ.sd,GG.sd)
results[ 1, 5] <- Perm.Test(SQ.x,FC.x,SQ.sd,FC.sd)
results[ 2, 3] <- Perm.Test(AC.x,SR.x,AC.sd,SR.sd)
results[ 2, 4] <- Perm.Test(AC.x,GG.x,AC.sd,GG.sd)
results[ 2, 5] <- Perm.Test(AC.x,FC.x,AC.sd,FC.sd)
results[ 3, 4] <- Perm.Test(SR.x,GG.x,SR.sd,GG.sd)
results[ 3, 5] <- Perm.Test(SR.x,FC.x,SR.sd,FC.sd)
results[ 4, 5] <- Perm.Test(GG.x,FC.x,GG.sd,FC.sd)
```

```
# write out results to CSV text file
write.table(results,file="results.csv",sep=",")

# transform results into suitable object for clustering procedures
distresults <- as.dist(results)

# cluster distance values using average method
hcresults <- hclust(distresults, method ="average")

# calculate cophenetic values
hcoph <- cophenetic(hcresults)

# calculate cophenetic correlation coefficient
hcor <- cor(distresults,hcoph)

# plot dendrogram with various labels
plot(hcresults, hang=-1,main="Tasmania samples",xlab="Average method",
sub=paste("Cophenetic correlation:",format(hcor,digits=2)), ylab="Functional
estimate distance")
```

Appendix B. Laser ablation isotopic zircon dating

Laser ablation isotopic dating of the Ovens Graben samples was conducted by a pulsed ArF LambdaPhysik LPX 120I UV excimer laser operated at a constant voltage between 21 and 23 kV at 5Hz. The spot diameter was 29 μm. The ablated material was carried by He–Ar gas mixture from a custom-designed sample cell and flow homogenizer to a Fissions VG PlasmaQuad II+ICP-MS. Raw count rates for ^{10}B, ^{29}Si, ^{32}P, ^{96}Zr, ^{206}Pb, ^{207}Pb, ^{208}Pb, ^{232}Th and ^{238}U were collected in time-resolved mode. ^{204}Pb was not measured because of a relatively high ^{204}Hg background. The integration time for the three Pb isotopes was 102.4 ms, whereas for the other isotopes it was 20.48 ms sampling at 1 point per peak. Data were acquired for 20 s with the laser off and 40 s with the laser on, giving~120 mass scans for a penetration depth of ~20 μm.

Corrections were made for mass bias drift, isotopic fractionation and common-Pb. After triggering the laser it took three to four mass scans for the counts to reach a steady signal so these initial datawere excluded. Depth-dependent inter-element fractionation of Pb, Th, and U (e.g. Hirata and Nesbitt, 1995; Horn et al., 2000) were corrected by reference to standard zircon CZ3 (Nelson, 1997). Measured ^{207}Pb/^{206}Pb, ^{206}Pb/^{238}U and ^{208}Pb/^{232}Th ratios in CZ3 were averaged over the course of the analytical session to calculate correction factors. These correction factors were then applied to each sample to simultaneously correct for instrument mass bias and depth-dependent elemental and isotopic fractionation. Common Pb was subtracted after corrections and based on the difference between the measured and expected ^{208}Pb/^{206}Pb given measured ^{208}Pb/^{232}Th according to the methods of Compston et al. (1984). Unknown samples were analysed sequentially with standard zircon CZ3 (564 Ma, 550 ppm U; Nelson, 1997) and standard silicate glass NIST SRM 612 (Pearce et al., 1997). Data are excluded from further provenance interpretation based on the degree of discordance (5%) and ratio variability across scans (MSWD: 10).

Table B1
Univariate U–Pb age data (age and 1σ uncertainty in Ma) for Ovens Graben samples

JRA		JRB		URA	
x	σ	x	σ	x	σ
378.5	1.5	292.8	3.8	290.8	1.2
388.2	1.5	367.4	1.7	302.7	2.1
393.1	1.4	370.1	0.9	303.1	1.6
394.4	1.1	370.8	1.2	326.6	1.9
410.7	1.1	384.2	2.4	364.0	1.2
413.5	2.5	385.1	2.5	369.1	1.5
416.9	1.5	386.1	3.3	385.2	2.1
419.5	1.9	389.3	1.0	386.8	1.3
423.2	2.6	389.5	2.6	406.8	1.4
423.5	1.8	389.7	1.3	407.6	1.8
426.8	1.5	397.0	1.5	407.9	1.5
429.9	0.9	403.4	1.2	411.5	2.7
431.6	3.0	408.6	2.0	412.6	3.3
432.6	7.1	409.9	1.9	415.0	1.7

(continued on next page)

Table B1 (*continued*)

JRA		JRB		URA	
x	σ	*x*	σ	*x*	σ
432.7	1.8	410.0	2.0	419.0	1.4
433.5	2.3	412.3	1.3	426.3	1.7
433.8	1.9	415.2	1.8	431.2	1.4
435.4	3.3	417.5	2.9	432.6	1.2
441.0	1.9	419.4	1.0	443.5	2.4
441.6	2.9	420.3	2.2	451.4	1.2
444.9	2.9	424.3	1.4	505.0	1.9
450.0	2.4	424.7	2.6	520.5	2.8
451.9	2.9	426.1	2.1	523.9	1.9
453.5	1.7	430.6	1.7	611.5	2.8
453.9	1.9	432.9	1.8	639.0	1.7
477.8	2.5	441.2	1.8	749.1	2.4
489.0	3.1	463.8	3.4	853.8	4.8
493.4	1.7	486.5	1.9	863.7	2.4
494.2	2.5	487.0	2.1	1027.6	3.2
499.2	3.2	487.5	2.1	1102.6	17.3
504.0	1.5	499.7	1.5	1155.7	4.0
507.1	2.3	504.6	1.8	1180.6	4.7
508.2	2.0	505.3	2.5	2808.8	7.0
510.5	3.1	506.5	1.4		
526.0	1.7	507.9	3.1		
558.0	2.6	545.0	2.0		
602.9	2.3	568.9	2.0		
603.5	2.7	570.1	1.7		
623.6	1.9	590.5	2.6		
631.3	3.1	591.2	3.0		
632.3	4.2	592.6	2.6		
990.6	5.6	995.9	2.9		
1032.9	2.6	1106.6	2.3		
1046.4	5.0	1158.0	9.0		
1138.5	8.2	1158.5	5.2		
1717.9	8.4	1211.8	5.3		
2406.8	5.6	1651.2	28.9		
2469.7	12.0	1679.5	5.7		
2505.8	6.1	1765.3	5.2		
		1802.8	6.5		

JRA: Jerilderie-A; JRB: Jerilderie-B; URA: Urana.

References

Berry, R.F., Jenner, G.A., Meffre, S., Tubrett, M.N., 2001. A North American provenance for Neoproterozoic to Cambrian sandstones in Tasmania. Earth and Planetary Science Letters 192, 207–222.

Black, L.P., Seymour, D.B., Corbett, K.D., Cox, S.E., Streit, J.E., Bottrill, R.S., Calver, C.R., Everard, J.L., Green, G.R., McClenaghan, M.P., Pemberton, J., Taheri, J., Turner, N.J, 1997. Dating Tasmania's oldest geological events. Australian Geological Survey Organisation Record 1997/15.

Brandon, M.T., 1992. Decomposition of fission track grain age distributions. American Journal of Science 292, 535–564.

Brandon, M.T., Vance, J.A., 1992. New statistical methods for analysis of FT grain age distributions with applications to detrital zircon ages from the Olympic subduction complex, western Washington State. American Journal of Science 292, 565–636.

Burrett, C., Berry, R., 2002. A statistical approach to defining Proterozoic crustal provinces and testing continental reconstructions of Australia and Laurentia—SWEAT or AUSWUS? Gondwana Research 5, 109–122.

Camacho, A., Hensen, B.J., Armstrong, R., 2002. Isotopic test of thermally driven intraplate orogenic model, Australia. Geology 30, 887–890.

Cawood, P.A., Nemchin, A.A., 2000. Provenance record of a rift basin: U/Pb ages of detrital zircons from the Perth Basin, Western Australia. Sedimentary Geology 134, 209–234.

Compston, W., Williams, I.S., Meyer, C., 1984. U–Pb geochronology of zircons from lunar breccia 73217 using sensitive high mass-resolution ion microprobe. Journal of Geophysical Research 89, B525–B534.

Cox, R., Armstrong, R.A., Ashwal, L.D., 1998. Sedimentology, geochronology and provenance of the Proterozoic Itremo Group, central Madagascar, and implications for pre-Gondwana palaeoceanography. Journal of the Geological Society (London) 155, 1009–1024.

Davis, J.C., 1986. Statistics and Data Analysis in Geology, 2nd ed. John Wiley & Sons, New York.

DeGraaff-Surpless, K., Mahoeney, B., Wooden, J., McWilliams, M., 2003. Lithofacies control in detrital zircon provenance studies: insights from the Cretaceous Methow Basin, southern Canadian Cordillera. Geological Society of America Bulletin 115, 899–915.

Edgington, E.S., 1987. Randomization Tests. M. Dekker, New York.

Fedo, C.M., Sircombe, K.N., Rainbird, R.H., 2003. Detrital zircon analysis of the sedimentary record. In: Hanchar, J.M., Hoskin, P.W.O. (Eds.), Zircon. Reviews in Mineralogy and Geochemistry, vol. 53. pp. 277–303.

Gehrels, G.E., 2000. Introduction to detrital zircon studies of Paleozoic and Triassic strata in western Nevada and northern California. In: Soreghan, M.J., Gehrels, G.E. (Eds.), Paleozoic and Triassic Paleogeography and Tectonics of Western Nevada and Northern California, Geological Society of America Special Paper, vol. 347. pp. 1–17.

Gehrels, G.E., Stewart, J.H., Ketner, K.B., 2002. Cordilleran-margin quartzites in Baja California—implications for tectonic transport. Earth and Planetary Science Letters 199, 201–210.

Gordon, A.D., 1999. Classification. Chapman & Hall, Boca Raton.

Grunsky, E.C., 2002. R: a data analysis and statistical programming environment—an emerging tool for geosciences. Computers & Geosciences 28, 1219–1222.

Hallsworth, C.R., Morton, A.C., Claoué-Long, J., Fanning, C.M., 2000. Carboniferous sand provenance in the Pennine Basin, UK: constraints from heavy mineral and detrital zircon age data. Sedimentary Geology 137, 147–185.

Hartigan, J.A., 1975. Clustering Algorithms. Wiley, New York.

Hirata, T., Nesbitt, R.W., 1995. U–Pb isotope geochronology of zircon: evaluation of the laser probe-inductively coupled plasma mass spectrometry technique. Geochimica et Cosmochimica Acta 59, 2491–2500.

Horn, I., Rudnick, R.L., McDonough, W.F., 2000. Precise elemental and isotope ratio determination by simultaneous solution nebulization and laser ablation-ICP-MS: application to U–Pb geochronology. Chemical Geology 164, 281–301.

Ihaka, R., Gentleman, R., 1996. R: a language for data analysis and graphics. Journal of Computational and Graphical Statistics 5, 299–314.

Ireland, T.R., Flöttman, T., Fanning, C.M., Gibson, G.M., Preiss, W.V., 1998. Development of the early Paleozoic Pacific margin of Gondwana from detrital zircon ages across the Delamerian orogen. Geology 26, 243–246.

Kearey, P., Brooks, M., 1991. An Introduction to Geophysical Explorations. Blackwell Scientific Publications, London.

Nelson, D.R., 1997. Compilation of SHRIMP U–Pb zircon geochronology data 1996. Geological Survey of Western Australia Record 1997/2.

Pearce, N.J.G., Perkins, W.T., Westgate, J.A., Gorton, M.P., Jackson, S.E., Neal, C.R., Chenery, S.P., 1997. A compilation of new and published data for NIST SRM 610 and NIST SRM 612 glass reference materials. Geostandards Newsletter 21, 115–144.

Press, W.H., Teukolosky, S.A., Vetterling, W.T., Flannery, B.P., 1988. Numerical Recipes in C: The Art of Scientific Computing. Cambridge Univ. Press, Cambridge.

Rainbird, R.H, Stern, R.A., Khudoley, A.K., Kropachev, A.P., Heaman, L.M., Sukhorukov, V.I., 1998. U–Pb geochronology of Riphean sandstone and gabbro from southeast Siberia and its bearing on the Laurentia–Siberia connection. Earth and Planetary Science Letters, 409–420.

Sambridge, M.S., Compston, W., 1994. Mixture modelling of multi-component data sets with application to ion-probe zircons. Earth and Planetary Science Letters 128, 373–390.

Silverman, B.W., 1986. Density Estimation for Statistics and Data Analysis. Chapman & Hall, London.

Sircombe, K.N., 1999. Tracing provenance through the isotope ages of littoral and sedimentary detrital zircon, eastern Australia. Sedimentary Geology 124, 47–67.

Sircombe, K.N., 2000. Quantitative comparison of large sets of geochronological data using multivariate analysis: a provenance study example from Australia. Geochimica et Cosmochimica Acta 64, 1593–1616.

Sircombe, K.N., 2004. AgeDisplay: an EXCEL workbook to evaluate and display univariate geochronological data using binned frequency histograms and probability density distributions. Computers & Geosciences 30, 21–31.

Sneath, P.H.A., Sokal, R.R., 1973. Numerical Taxonomy: The Principles and Practice of Numerical Classification. W. H. Freeman, San Francisco.

Stefanski, L., Carroll, R.J., 1990. Deconvoluting kernel density estimators. Statistics 21, 169–184.

Swan, A.R.H., Sandilands, M., 1995. Introduction to Geological Data Analysis. Blackwell Science, Oxford.

Veevers, J.J., 1984. Phanerozoic Earth History of Australia. Oxford Science Publishers, Oxford.

Veevers, J.J., 2000. Antarctic Beardmore-Ross and Mirny provenances saturate Paleozoic–Mesozoic East Gondwanaland with 0.6–0.5 Ga zircons. In: Veevers, J.J. (Ed.), Billion-year earth history of Australia and neighbours in Gondwanaland. Gemoc Press, Sydney.

Wand, M.P., Jones, M.C., 1995. Kernel Smoothing. Chapman & Hall, London.